Interaction of near-field microscopy probes with surface plasmon polaritons

2017 J. Opt. 19 055005

(http://iopscience.iop.org/2040-8986/19/5/055005)

IOP Publishing Journal of Optics
J. Opt. **19** (2017) 055005 (6pp) https://doi.org/10.1088/2040-8986/aa68fa

Interaction of near-field microscopy probes with surface plasmon polaritons

Cesar E Garcia-Ortiz[1], **Luis Santamaria**[2] and **Hector R Siller**[2]

[1] CONACYT—CICESE, Unidad Monterrey, Alianza Centro 504, PIIT Apodaca, 66629, Mexico
[2] Tecnológico de Monterrey, Eugenio Garza Sada 2501 Sur, Monterrey, N.L., 64849, Mexico

E-mail: cegarcia@cicese.mx

Received 11 January 2017, revised 21 March 2017
Accepted for publication 24 March 2017
Published 18 April 2017

Abstract

In this work, we use a collection-type scanning near-field optical microscope to study the intensity distribution along the direction perpendicular to the interface, considering the interaction of the probe with the evanescent field of surface plasmon polaritons. A decrease of the signal is observed as the probe comes near to contact, as opposed to the expected single exponential increase. This effect is explained with a relatively simple semi-analytical model that takes into account the shape of the tip and the geometrical cutoff of the plasmonic mode. The proposed model confirm the presence of the intensity dip near the surface, as a result of the perturbation of the field caused by the probe.

Keywords: near field, plasmonics, SNOM

(Some figures may appear in colour only in the online journal)

1. Introduction

Scanning near-field optical microscopy (SNOM) is an imaging technique that is capable of detecting the signal of non-radiative (evanescent) electromagnetic fields [1]. Depending on the detection technique, SNOMs can be divided in two main categories: collection and scattering types. The scattering type, s-SNOM, usually consists of a tapered tip that is scanned over the sample of interest and oscillates at its resonance frequency. The tip, which can be coated or uncoated, scatters the optical near-field signal. The scattered light is proportional to the evanescent field, and the signal can be measured in a detector by using, for example, an objective lens [2]. In collection mode, the probe (usually a tapered optical fiber) is scanned over the sample of interest, and the evanescent field couples into the subwavelength-sized tip of the probe. The mode propagates along the tip and couples into the guided mode of the fiber. The other end of the fiber is connected to a detector to measure the transmitted signal [3].

Surface plasmon polaritons (SPPs) are collective oscillations of the electrons in a metal at the surface of a metal–dielectric interface [4]. The field associated to SPPs is evanescent, i.e. the field decays exponentially as it penetrates into the dielectric. There are several techniques to excite SPPs, such as prism coupling [5, 6], gratings [7], and subwavelength surface defects [8], among others. One of the most used techniques consists of the Kretschmann configuration [5]. This technique uses the principle of total internal reflection to couple the evanescent field into SPPs, by tuning the magnitude of the wavevector by changing the angle of incidence. SNOM can be used to image the intensity distribution of SPPs. Nevertheless, the effect of bringing the tip to close proximity with the sample can modify the field itself perturbing it. Several studies have focused on the effect of the probe-sample interaction by considering the tip as a dipole [9]. This approach explains the local field distributions in the presence of the probe, but fails to predict the signal that is transmitted into a fiber in collection mode.

In this work, we use a collection type SNOM to measure the intensity decay along the direction perpendicular to the interface. A decrease of the signal is observed as the probe comes near to contact, as opposed to the expected single exponential increase. This effect is explained with a relatively simple approach that takes into account the shape of the tip and the geometrical cutoff of the metal–dielectric SPP mode. Our numerical simulations confirm the presence of the intensity dip near the surface, and the signal response for

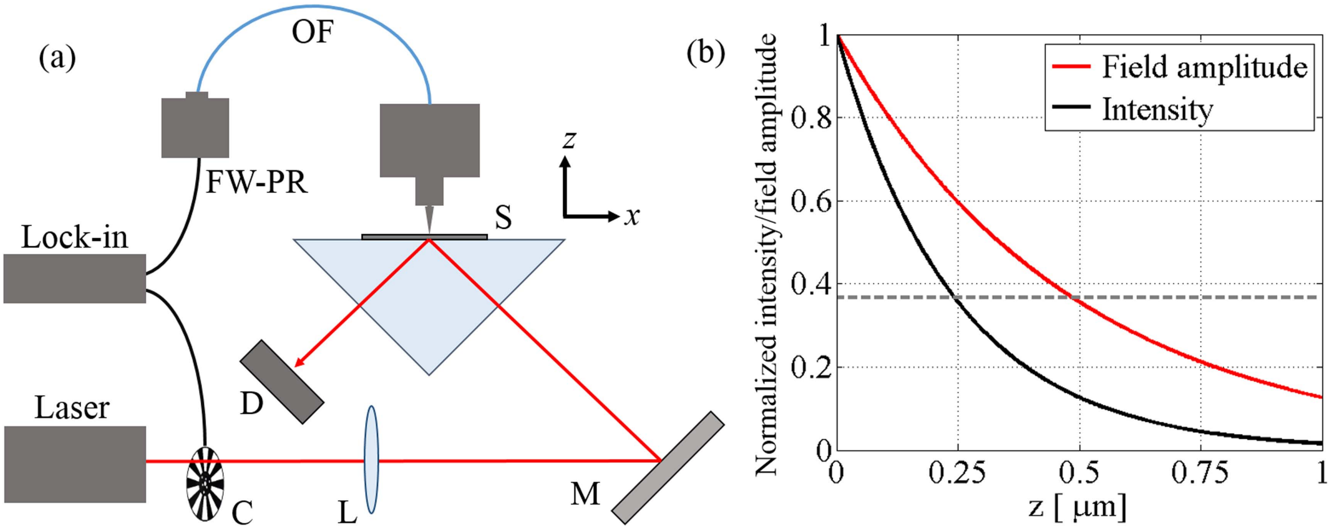

Figure 1. (a) Experimental setup consisting of a Kretschmann configuration. The setup uses a lens (L) to focus onto the sample (S). The incidence angle can be adjusted using the mirror (M). The reflected light is measured with a power meter (D). The detected signal is transmitted through an optical fiber (OF) and detected with a femtowatt photoreceiver (FW-PR). (b) Field amplitude and intensity of the normal component of an SPP as a function of the distance from the surface. The dashed line indicates the $1/e$ value.

different geometries and parameters are calculated and analyzed.

2. Materials and methods

2.1. Experimental setup

The sample consists of a 70 nm thick gold film evaporated over a glass substrate. The sample is situated onto one of the faces of a 45° BK7 ($n = 1.512$) prism using refractive index matching oil. The experimental setup is a usual configuration of the Kretschmann setup. To excite the SPPs, we use a Ti: Sapphire laser, tuned at a wavelength $\lambda_0 = 740$ nm. The laser beam is focused into the sample using a lens of long focal length $f = 1$ m, and the incidence angle is adjusted using a mirror (figure 1(a)). The reason to choose such a long focal distance is to generate a beam with a sufficiently large Rayleigh range, to consider it almost as a plane wave in the focus. The probes used in this experiments are tapered optical fibers, chemically etched using the Turner method [9]. The fibers have a radius of curvature of ~150 nm, and a conical angle $\theta = 20°$. We use a power detector to measure the reflected light of the laser beam after passing through the prism to find the SPP resonance angle (~42.8°). The laser light was modulated using a mechanical chopper, and the signal was detected using a femtowatt photoreceiver, which is connected to a lock-in amplifier.

2.2. The SPP penetration depth

The normal component of the electric field of an SPP that propagates in the x-direction along a metal–air interface can be described by $\mathbf{E}_z(x,\ z) = E_{0z}\ \exp[\mathrm{i}(\beta x + k_{zi}\ z)]\hat{\mathbf{z}}$, where $\beta = k_0\sqrt{\varepsilon_m/(\varepsilon_m + 1)}$ is the propagation constant of the SPP mode, k_0 is the free-space wavevector, E_{0z} is the amplitude of the incident field, ε_m is the dielectric functions of the metal, and k_{zi} is the wavevector in the direction perpendicular to the interface ($i = m$, or d, into the metal and dielectric, respectively). One can solve the boundary conditions to find the expressions of each the normal wavevectors, $k_{zd}^2 = \beta^2 - k_0^2$, and $k_{zm}^2 = \beta^2 - \varepsilon_m k_0^2$. The distance, normal to the interface, where the field amplitude drops $1/e$ times is known as the penetration depth (a.k.a. decay length or skin depth), and can be expressed as $\delta_i = 1/|k_{zi}|$. In practice, detectors give a measurement of the intensity, so we define also an intensity penetration depth, where the intensity has dropped $1/e$ of its original value, given by $\gamma_i = 1/|2k_{zi}|$. Using these equations, we find the field and intensity penetration depths into the dielectric, in an air–gold ($\varepsilon_m = -17 + 1.45\mathrm{i}$) interface at a wavelength $\lambda_0 = 740$ nm. The field and intensity penetration depths are $\delta_d = 483$ nm and $\gamma_d = 241$ nm (figure 1(b)).

2.3. SPP geometrical cutoff

In this section, we consider a four-layer system formed by glass, gold, air, and silica (figure 2(a)). The air gap has a thickness g, and is in the middle between the gold film of thickness $t = 70$ nm, and a semi-infinite dielectric medium ($n_c = 1.457$). The substrate is also considered semi-infinite, and has a refractive index $n_s = 1.512$. We solve the four-layer system using a semi-analytical approach [10], by finding the corresponding complex eigenvalues that satisfy the boundary conditions. Complementary information of four-layer plasmonic systems can be found in [11–13]. For sufficiently large air gaps ($g > 3\lambda$), the gold–air mode is not affected by the presence of another medium, but as g decreases, the mode will necessarily disappear at some point, due to a mismatch of wavevectors in the Kretschmann configuration. The system is solved while varying the air gap thickness to determine the values for which the gold–air SPP mode exists (figure 2(a)).

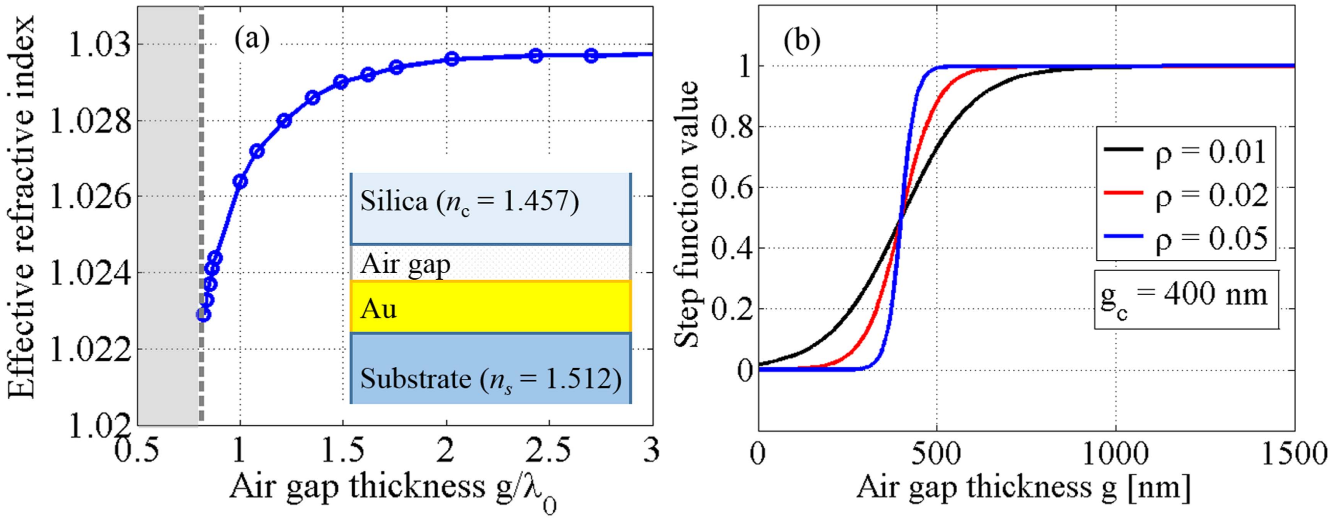

Figure 2. (a) Effective refractive index of the SPP mode dependence on the air gap thickness g. The gray area indicates the geometrical cutoff of the SPP mode. (b) Logistics function used as a smooth step function.

This eigenvalue problem consists in finding the complex effective refractive index n_{eff} of the plasmonic mode. There are several possible solutions for this system, but in this section we will consider only the evolution of the solution of the mode associated to the gold–air SPP mode as the air gap is decreased, starting from $g = 3\lambda_0$ to $0.5\lambda_0$ (1220–370 nm). When the air gap gets smaller, the effective index decreases as a result of the presence of the approaching layer. The calculation shows that the real part of n_{eff} decreases slowly in the interval from $g = 3$ to $1.5\lambda_0$. For lower values of g, the SPP mode becomes leaky and has a cutoff value $g_c \sim 0.8\lambda_0$ ($\sim$590 nm), i.e. for air gaps smaller than g_c, it is not further possible to find a bound solution in the gold–air interface.

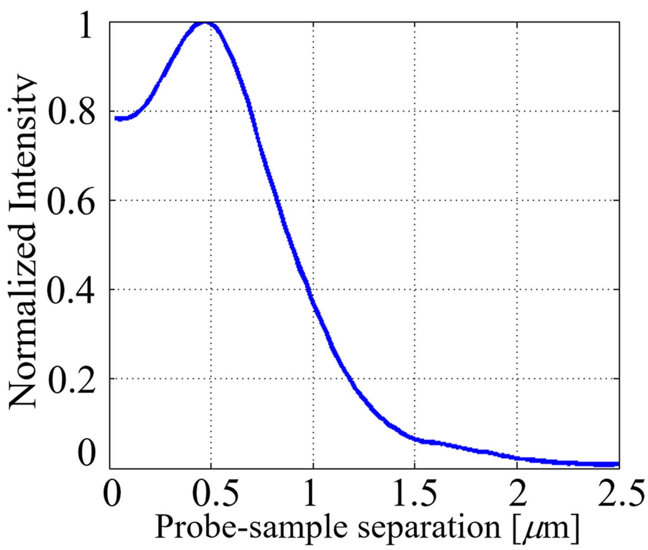

Figure 3. Normalized optical signal measured along the direction normal to the interface.

3. Results and discussion

3.1. Experimental results

The experiment consists of measuring the intensity decay along the direction normal to the interface of the gold–air SPP at a wavelength $\lambda_0 = 740$ nm. The tip of the SNOM probe is positioned in the shear-force region ($\sim$10 nm from the surface), and moved apart while simultaneously measuring the intensity of the signal. Instead of detecting an exponential decay, the measured signal showed an increase of the intensity as the probe was moved away from the surface within a range of $\sim$400 nm above the sample. After this point, the intensity reaches a maximum and then starts to decay (figure 3). This effect was observed in every repetition of the experiment. To verify this behavior, we changed the position where the laser was focused, and realigned the mirror which controls the angle of incidence, with no change of the experimental result. After the probe has been moved apart of the surface more than 1 μm, the signal shows a well-defined exponential decay. If we measure the penetration length neglecting the signal before 1 μm, we get a value of 287 nm, which is in good agreement with the theoretical prediction obtained in section 2.2. In this sense, we are confident that the detected signal corresponds to the near-field detection of SPPs. The intensity behavior below 1 μm, may be explained by the perturbation of the field caused by the probe. In the next section, we describe a model we developed to understand this phenomenon based on the influence of the presence of the tip, and the geometrical parameters, such as the radius of curvature and the conical angle of the fiber tip.

3.2. Numerical calculations and model

The proposed model considers that the gold–air SPP does not exist if the probe-sample distance is below the geometrical cutoff obtained in section 2.3. To get a smooth cutoff of the field distribution in space, and avoid unphysical singular

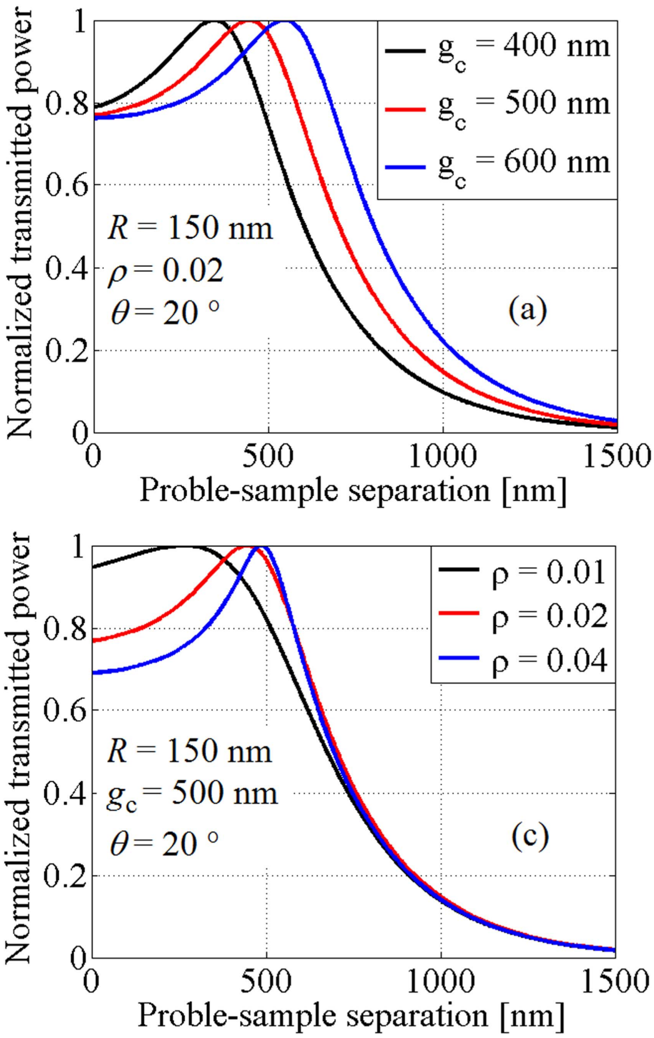

Figure 4. Transmitted power into the probe as a function of the probe-sample separation when varying (a) the geometrical cutoff, (b) the radius of curvature, (c) the smoothening parameter of the step function, and (d) the conical angle of the probe.

behaviors of the field, we use the logistics function

$$\varphi(\alpha;\, \rho,\, \alpha_0) = \frac{1}{1 + \mathrm{e}^{-\rho(\alpha-\alpha_0)}}, \tag{1}$$

as a smooth step function (figure 2(b)) [14]. The parameter ρ defines the smoothness, or slope, of the function, and α_0 is the position of the step. For our purposes, the position of the step is the cutoff value of the air gap ($\alpha_0 = g_c$). The objective is to simulate the SPP field in the presence of the probe, considering the geometrical cutoff of the mode, to estimate the intensity of the signal as a function of the probe-sample distance. Bearing this in mind, it is evident that the shape of the tip influences how the signal is collected. We model the shape of the tip with a hyperbola described by

$$V(x,\, h) = b\sqrt{1 + \frac{x^2}{a^2}} + (h - b), \tag{2}$$

where h is the probe-sample distance of separation, and a and b are geometrical parameters that are related to the conical angle of the fiber as $a = b\tan\theta$, and to the radius of curvature R of the tip. Mathematically, is not possible to find a single radius of curvature of a hyperbola, so we use the approximation $R = 2(f - b)$, where f is the focus of the hyperbola defined as $f^2 = a^2 + b^2$. Now, we can describe the transmitted power of the SPP field that couples into the fiber by integrating the intensity distribution of the projection of the normal component of the SPP field in the boundaries of the fiber, to get

$$T(h) = \iint_S \varphi[V(r,\, h);\, \rho,\, g_c]\ \|\mathbf{E}_z[0,\quad V(r,\, h)]\cdot\hat{\mathbf{n}}\|^2\,\mathrm{d}A, \tag{3}$$

assuming that the SPP field is invariant in the x-direction in the absence of the tip. The integral is solved numerically along the surface S, which is a hyperboloid of revolution obtained by rotating V around the z-axis. Integrating, we get a distribution of the transmitted power as a function of the probe-sample separation distance.

The obtained results show that the presence of the probe modifies the simple exponential decay that SPPs have in the normal direction to the interface (figure 4). The transmitted power does not have its maximum value when the probe is in contact with the surface, but near the value of g_c. We performed the calculations varying g_c, R, ρ, and θ to observe

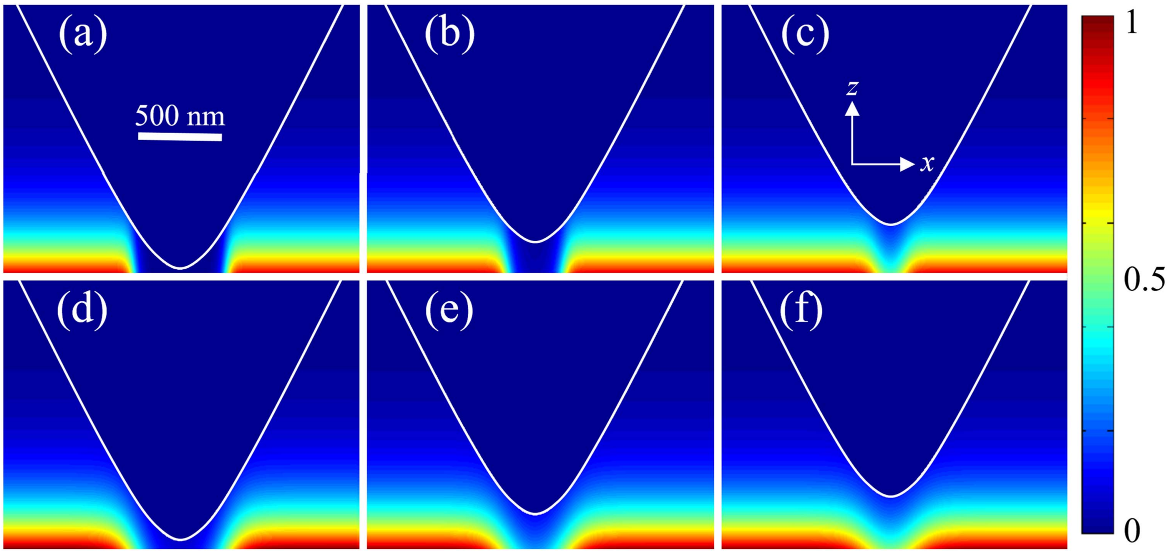

Figure 5. Intensity distribution of the SPP in the presence of the tip for different probe-sample separation distances, $h = 50$, 200, 300 nm. In (a)–(c) the smoothening parameter is $\rho = 0.03$, and in (d)–(f) is set to 0.01.

their effect in $T(h)$ (figures 4(a)–(d)). All the combinations show slight differences in the behavior of the transmitted power before g_c, but the dip is present in most of the cases. The situations that do not resemble the experimental result, occurs when the parameters differ far from the real tip ($R = 50$ nm, and $\theta = 40°$). Also an excessive smoothening of the cutoff yields a different results, and the best fit is found for $\rho = 0.03$. Using the obtained numerical results (ρ and g_c) and the proposed model, we can evaluate the z-component of the SPP field intensity in the xz plane to get a better visualization on how the tip modifies the field (figure 5). Figure 5 shows the intensity maps for different probe-sample separation distances, and is constructed considering the interaction of the probe with the SPPs by using the expression $I_z(x, z) = E_z(x, z) \cdot \varphi[V(x, h); \rho, g_c]$. When h is small ($\sim$50 nm), the mode amplitude is strongly reduced below the tip (figures 5(a) and (d)), and the main contributors to the transmitted signal is due to the coupling through the lateral walls. As the probe is separated from the surface, the mode appears gradually and the transmitted power increases.

4. Conclusions

We have proposed a model to describe the SPP-probe interaction in a collection type SNOM, which explains the evolution of the measured signal as a function of the probe-sample separation distance. The calculated values of the model are in good agreement with the results obtained experimentally. The transmitted power of the SPPs coupled into the probe, has a strong dependence on the geometrical parameters of the tip, and we find that for some cases the maximum transmitted power is not measured when the tip is in contact with the surface, but close to the value of the geometrical cutoff. These results stress the importance of considering the interaction of the probe with the SPP field, and show how the perturbation depends on the separation distance, and on the shape and material of the probe.

Acknowledgments

We acknowledge the financial support from CONACYT Basic Scientific Research Grant No. 242634, and CONACYT scholarship No. 661876. We also thank V A Zenin and V Coello for fruitful discussions in the subject.

References

[1] Bozhevolnyi S 2000 Near-field optics of nanostructured surfaces *Optics of Nanostructured Materials* ed V A Markel and T F George (New York: Wiley)
[2] Zenin V A, Andryieuski A, Malureanu R, Radko I P, Volkov V S, Gramotnev D K, Lavrinenko A V and Bozhevolnyi S I 2015 Boosting local field enhancement by on-chip nanofocusing and impedance-matched plasmonic antennas *Nano Lett.* **15** 8148
[3] Bozhevolnyi S I, Volkov V S and Leosson K 2002 Localization and waveguiding of surface plasmon polaritons in random nanostructures *Phys. Rev. Lett.* **89** 186801
[4] Maier S 2007 *Plasmonics: Fundamentals and Applications* (Berlin: Springer)
[5] Kretschmann E 1971 Die bestimmung optischer konstanten von metallen durch anregung von oberflächenplasmaschwingungen *Z. Phys.* **241** 313
[6] Otto A 1968 Excitation of nonradiative surface plasma waves in silver by the method of frustrated total reflection *Z. Phys.* A **216** 398
[7] Ditlbacher H, Krenn J R, Hohenau A, Leitner A and Aussenegg F R 2003 Efficiency of local light-plasmon coupling *Appl. Phys. Lett.* **83** 3665
[8] Baudrion A-L, de Leon-Perez F, Mahboub O, Hohenau A, Ditlbacher H, Garcia-Vidal F J, Dintinger J, Ebbesen T W, Martin-Moreno L and Krenn J R 2008 Coupling efficiency of light to surface plasmon polariton for single subwavelength holes in a gold film *Opt. Express* **16** 3420

[9] Esslinger M and Vogelgesang R 2012 Reciprocity theory of apertureless scanning near-field optical microscopy with point-dipole probes *ACS Nano* **6** 8173
[10] Baltar H T, Drozdowicz-Tomsia K and Goldys E M 2012 Propagating surface plasmons and dispersion relations for nanoscale multilayer metallic-dielectric films *Plasmonics—Principles and Applications* ed K Y Kim (Rijeka: InTech)
[11] Stiens J, Vounckx R, Veretennicoff I, Voronko A and Shkerdin G 1997 Slab plasmon polaritons and waveguide modes in four-layer resonant semiconductor waveguides *J. Appl. Phys.* **81** 1
[12] Sikdar D and Kornyshev A A 2016 Theory of tailorable optical response of two-dimensional arrays of plasmonic nanoparticles at dielectric interfaces *Sci. Rep.* **6** 33712
[13] Shaidiuk V and Menabde S G 2016 Modal evolution in asymmetric three- and four-layer plasmonic waveguides *Opt. Express* **24** 16595
[14] Iliev A I, Kyurkchiev N and Markov S 2015 On the approximation of the cut and step functions by logistic and gompertz functions *Biomath* **4** 1–12